Infusion of Polymer into a Porous Glass Bead As Studied by Space-Resolved Jamin Interferometry

Anil Dube and Iwao Teraoka*

Department of Chemical Engineering, Chemistry, and Materials Science, Polytechnic University, 333 Jay Street, Brooklyn, New York 11201

Received March 25, 1997; Revised Manuscript Received June 30, 1997[⊗]

ABSTRACT: Jamin interferometry was applied to a porous glass bead in order to observe transient infusion of solvated polymer into the medium after the polymer was added to the surrounding solvent. Analysis of the fringe pattern along the equator of the bead image allowed us to obtain the concentration profile of the polymer at different times during the infusion. It was found that there are some polymer chains that quickly enter the pores and spread throughout the medium. Afterward, the concentration profile slowly approached an equilibrium uniform distribution. When the polymer chain's dimension was smaller than the pore size, the approach was limited by intrapore diffusion of the chains. In contrast, the entrance of polymer chains into the pores near the bead surface was rate-limiting for polymer chains with a dimension larger than the pore size. The rate of entrance increased at higher concentrations. Unlike studies of transport through a porous membrane, space-resolved interferometry of the porous glass has the advantage of being able to distinguish the entrance from the intrapore diffusion.

Introduction

It often happens that a polymer system, when a geometrical restriction is imposed, exhibits properties unavailable in the bulk system.[1] For instance, gel permeation chromatography (GPC) utilizes the dependence of the equilibrium partition coefficient, defined as the ratio of the polymer concentration in a porous medium to that in the surrounding solution, on the chain dimension.[2] In gel electrophoresis, charged polymer chains are separated by the difference in the electrophoretic mobility in a cross-linked matrix polymer.

To study the partitioning, especially at higher concentrations, we constructed[3] a Jamin interferometer. A porous silica bead was immersed into a solution of polymer. When equilibrium was reached, an interferogram was recorded. Digital image analysis of the interferogram allowed us to estimate the concentration of the polymer in the interior of the silica bead. In our first contribution,[3] we reported on the measurement of an equilibrium partition coefficient, K, as a function of the concentration in the surrounding solution for different fractions of polystyrene standard. It was found that K increases with concentration and approaches unity, in agreement with the theories[4,5] that predict a weak-to-strong penetration transition, primarily because of the increased osmotic pressure of the polymer solution at higher concentrations. The increase, however, required a concentration higher than the one predicted by theory,[5] especially for low molar mass fractions.

After the first work, we found that the interferometry can be extended to the measurement of a spatial distribution of the polymer concentration in the interior of a silica bead. In particular, the spatial resolution is useful to observe infusion of polymer into the silica bead following an increase in the polymer concentration in a solution in which the bead is immersed. The rate of infusion determines the processing speed in some applications. In GPC, for instance, the linear velocity of the mobile phase has to be sufficiently low to allow concentration equilibrium between the stationary and mobile phases.

The infusion of polymer into a porous medium involves two processes. One is entrance of polymer chains into the medium through surface openings, and the other is permeation into the entire volume of the medium by intrapore diffusion. Transport of polymer molecules through porous membranes also involves entrance and intrapore diffusion.[1,6−10] For instance, the effective diffusion coefficient through the membrane is proportional to the product of K and the intrapore diffusion coefficient. It is difficult to distinguish the two processes in the membrane transport experiments, although the distinction is necessary in order to understand the transport on a molecular level.

Permeation by intrapore diffusion is related to diffusion processes studied intensively by Karasz and coworkers.[5,11−16] They applied dynamic light scattering to study various diffusion processes in a porous silica bead for polymer chains dissolved in a solvent that is isorefractive with silica. Diffusion of polymer in a gel matrix, a soft porous medium, also involves permeation. There have been extensive research activities in this area.[17−20]

Direct observation of the distribution of the concentration in a porous medium in general has been scarce, despite its obvious importance, for instance, in studies of the impregnation of chemical species into a porous medium and its release into the surroundings. Direct observation provides information on the transport of probe molecules in the porous medium at different locations in the medium. This information is unavailable to other techniques, such as dynamic light scattering, that assume uniform distribution of the probe molecules in the medium and trace their diffusional motions at equilibrium. To the authors' knowledge, only one group has obtained the spatial distribution of probe molecules. Recently, Schlick et al.[21,22] applied space-resolved electron-spin resonance spectroscopy to track the change in the concentration profile of tracer polymer molecules in a hydrogel. They found that the diffusion coefficient depends on the volume fraction of the gel matrix, and the dependence is described by the free-volume theory.

In this contribution, we report an application of the spatially resolved interferometry to studies of infusion of solvated polymer into a porous silica bead. Unlike

[⊗] Abstract published in *Advance ACS Abstracts,* August 15, 1997.

S0024-9297(97)00406-3 CCC: $14.00

in studies of membrane transport, direct observation of the concentration profile of the probe polymer made it possible to separate the entrance into the pore and the permeation in the medium. We will first explain the experimental technique, including the method of image analysis and some problems related to nonidealities of the porous medium. Then, we will show results of the spatial distribution of the polymer in various stages of infusion and discuss the rates of the entrance and the permeation.

Space-Resolved Jamin Interferometry

Earlier, we reported[3] Jamin interferometry to measure the concentration of a polymer in a porous silica bead equilibrated with a solution of the polymer. A spherical porous glass bead was immersed in a solution of a polystyrene standard of a given concentration, c_E, in a fluorometer cell. A laser beam of wavelength $\lambda = 632.8$ nm was split by a beam displacer into two vertically displaced, parallel beams. The top beam traveled the exterior solution, and the bottom beam illuminated the silica bead. The two beams were coupled by another beam displacer. The interference pattern was created by placing a polarizer in front of the projection screen. The pattern is illustrated in Figure 1a. The fringes were elliptic and displaced for the portion of the bead image, compared with the parallel fringes (period ξ) in the absence of the glass bead (background image). The largest displacement, Δx_m, was observed for the fringe at the center of the image.

The interior polymer concentration c_I was estimated by using the relationship[3]

$$(\lambda/d)(\Delta x_m/\xi) = (n_S - n_G)(1 - \rho) + (dn/dc)(c_E - \rho c_I) \quad (1)$$

where n_S and n_G are the refractive indexes of the pure solvent and silica, and dn/dc is the differential refractive index of the polymer solution. The porosity, ρ, defined as the fraction of the liquid-filled volume in the porous body, was measured separately by using mixtures of two liquids. The increment of the refractive index of the polymer solution with respect to the solvent was found to be proportional to the concentration. The diameter d was measured on the projection screen by rotating the cell by 90°. Use of a solvent (2-fluorotoluene at 42.0 °C) that is isorefractive with silica minimized the contribution of the first term on the right-hand side of eq 1, but it was usually nonzero and different from bead to bead. We evaluated the first term for the pure solvent ($c_E = 0$, and hence $c_I = 0$): $(\Delta x_m/\xi)_0 = (d/\lambda)(n_S - n_G)(1 - \rho)$. The difference in the reading of $\Delta x_m/\xi$ between the pure solvent and a solution of c_E was used to estimate c_I:

$$(\Delta x_m/\xi) - (\Delta x_m/\xi)_0 = (d/\lambda)(dn/dc)(c_E - \rho c_I) \quad (2)$$

The value of c_I thus determined is an average of the interior concentration along the light path through the bead center, in the event there is a concentration distribution. When the polymer infuses into a solvent-imbibed porous glass bead from the surrounding solution, for instance, it will create a spatial distribution in the concentration c_I, at least for short times. Examination of the fringe pattern will show how the polymer is transferred into the bead. In this contribution, we analyze the fringe pattern along a diameter of the bead image, taking advantage of the spherical symmetry of the bead. The procedure is explained below.

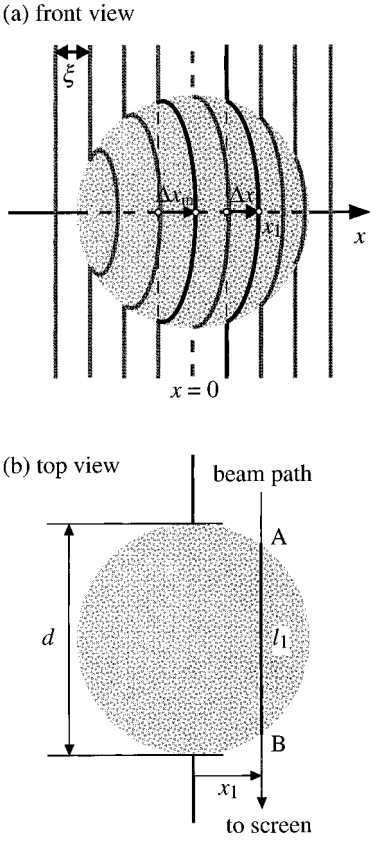

Figure 1. (a) Front view of a glass bead with an interference fringe pattern superimposed. (b) Top view of a glass bead.

In the front view (Figure 1a) of the porous glass bead, the laser beam propagates from the rear to the front of the paper. The x-axis runs along a diameter perpendicular to the exterior fringes with the origin at the bead center. One of the two photons that interfere at x_1 on the x-axis has passed the glass bead along AB $= l_1$, as indicated in the top view (Figure 1b). We define the refractive index $n_I(\mathbf{r})$ at $\mathbf{r}$ as its spatial average in a small volume that encompasses at least several pore sizes in the solution-filled glass bead. Note that, in the present system, the bead size is 5 orders of magnitude as large as the pore size. Then, $n_I(\mathbf{r})$ is written as

$$n_I(\mathbf{r}) = (1 - \rho(\mathbf{r}))n_G(\mathbf{r}) + \rho(\mathbf{r})[n_S + (dn/dc)c_I(\mathbf{r})] \quad (3)$$

where $\rho(\mathbf{r})$, $n_G(\mathbf{r})$, and $c_I(\mathbf{r})$ are defined for a similar volume. The other photon has passed the exterior solution that has a refractive index $n_E = n_S + (dn/dc)c_E$. If ρ and n_G are uniform in the porous medium, the optical path difference for the two photons is expressed as

$$\int_A^B [n_E - n_I(\mathbf{r})]\, d\mathbf{r} = l_1[(n_S - n_G)(1 - \rho) + (dn/dc)(c_E - \rho\overline{c_I})] \quad (4)$$

where the average of an arbitrary function, $X(\mathbf{r})$, is calculated along AB as $\bar{X} = \bar{X}(x_1) = (1/l_1)\int_A^B X(\mathbf{r})\, d\mathbf{r}$. If the cross section at the equator of the bead is circular, $l_1 = 2((d/2)^2 - x_1^2)^{1/2}$. When $c_I(\mathbf{r}) = c_I(|\mathbf{r}|)$ (spherical symmetry), $\overline{c_I}$ is expressed as

$$\overline{c_I}(x_1) = (2/l_1)\int_0^{l_1/2} c_I((x_1^2 + y^2)^{1/2})\, dy \quad (5)$$

The path difference in eq 4 is equal to $\lambda(\Delta x/\xi)$, where Δx is the displacement of the fringe at x_1 in the bead image with respect to the corresponding background

fringe. Comparison of $\Delta x/\xi$ between the measurements at $c_E = 0$ ($(\Delta x/\xi)_0$; a function of x_1) and at a nonzero c_E gives

$$(\Delta x/\xi) - (\Delta x/\xi)_0 = (l_1/\lambda)(dn/dc)(c_E - \rho\overline{c_I}) \quad (6)$$

At equilibrium, the concentration will be uniform, i.e., $c_I(\mathbf{r}) = c_{I,eq}$. Then eq 6 reads

$$(\Delta x/\xi)_{eq} - (\Delta x/\xi)_0 - (l_1/\lambda)(dn/dc)(c_E - \rho\overline{c_{I,eq}}) \quad (7)$$

At the center of the bead image ($x_1 = 0$), $l_1 = d$, and eq 7 reduces to eq 2. Comparison of eqs 2 and 7 allows us to estimate the thickness, l_1, of the glass bead as a function of x_1, in case there is a small deviation of the cross section from the circle. Then, by using eq 6, $\overline{c_I}(x_1)$ is obtained.

To deconvolute $\overline{c_I}(x_1)$ into $c_I(r)$, where $r = |\mathbf{r}|$, we first approximate $\overline{c_I}(x_1)$ by an even function of x_1/a, where $2a$ is the diameter on the x-axis and equals d for the circular cross section. If

$$c_I(r) = \zeta_0 + \zeta_2(r/a)^2 + \zeta_4(r/a)^4 + \zeta_6(r/a)^6 \quad (8)$$

for example, then eq 5 gives

$$\overline{c_I}(x_1) = \phi_0 + \phi_2(x_1/a)^2 + \phi_4(x_1/a)^4 + \phi_6(x_1/a)^6 \quad (9)$$

with $\phi_0 = \zeta_0 + (1/3)\zeta_2 + (1/5)\zeta_4 + (1/7)\zeta_6$, $\phi_2 = (2/3)\zeta_2 + (4/15)\zeta_4 + (6/35)\zeta_6$, $\phi_4 = (8/15)\zeta_4 + (8/35)\zeta_6$, and $\phi_6 = (16/35)\zeta_6$. Conversely, if $\overline{c_I}(x_1)$ is approximated by eq 9, $c_I(r)$ can be found as eq 8.

There are some nonideal factors to be considered in order to successfully estimate $c_I(r)$ from $\overline{c_I}(x_1)$: (1) the cross section of the glass bead at the equator may not be a circle; (2) the porosity may not be uniform; (3) the solid phase of the glass bead may have a nonuniform refractive index because of uneven distribution of minority components such as magnesia, borate, and alumina; (4) the pore size may not be uniform. In particular, the estimation will be affected by a radial variation of these quantities. As explained in the Appendix and shown below, the second nonideality was small in our experiments. The effect of the third factor, if any, was canceled by taking the difference between $\Delta x/\xi$ and $(\Delta x/\xi)_0$ in eq 6 (see Appendix). The fourth factor can be included in the distribution in c_I. Thus, we took account of the first factor only. It was corrected by using $(\Delta x/\xi)_{eq} - (\Delta x/\xi)_0$ as explained above.

Experimental Section

Porous Glasses. Porous glass beads S980A, supplied by Shell Chemical Co., were used. They have a bead diameter of ca. 2.3 mm, a pore radius R_p of 7.5 nm, a pore volume of 1.0 cm^3/g, and a surface area of 267 m^2/g. Surface silanol was replaced by trimethylsilanol to prevent adsorption of polymer as described elsewhere.[12] Beads L and M used here were found to have a porosity of 0.721 and 0.735, and a diameter of 2.20 and 2.14 mm, respectively. Measurement of the porosity was carried out by using the interferometer for the bead immersed in a mixture of cyclohexanone and 2-fluorotoluene (2FT) in various mixing ratios. The increment of the refractive index of the mixture with reference to cyclohexanone was obtained at $\lambda = 632.8$ nm as $\Delta n/(c_{2FT}/\text{wt}\%) = 2.212 \times 10^{-4}$ ($0 \le c_{2FT} \le 20.3$ wt %) at 25 °C, where c_{2FT} is the concentration of 2FT. See the literature for details.[3]

Samples. Characterization results for polystyrene standards purchased from Pressure Chemical are shown in Table 1. The peak molar mass, M_p, and the polydispersity index, M_w/M_n, where M_n and M_w are the number-average and weight-average molar masses, were obtained from the manufacturer. The radii of gyration, R_{g0}, in the dilute solution limit were calculated from the literature.[23] The overlap concentration, c^*, is defined as $c^*(2^{1/2}R_{g0})^3 = M_p/N_A$, where N_A is Avogadro's number. The partition coefficient, K_0, of an isolated polymer chain was calculated for a dilute solution of Gaussian chains of an equal R_{g0} equilibrated with a cylindrical pore of radius $R_p = 7.5$ nm. Reagent grade cyclohexanone and 2-fluorotoluene were purchased from Aldrich and used as received.

Table 1. Characterization of Polystyrene Fractions

polymer	M_p	M_w/M_n	R_g, nm	c^*, mg/mL	K_0
PS25K	25 470	1.06	5.3	102	3.9×10^{-2}
PS49K	48 900	1.06	7.7	62	1.7×10^{-3}
PS90K	89 300	1.04	10.9	41	3.1×10^{-6}
PS288K	293 000	1.06	21.4	18	3.1×10^{-21}

Differential Refractive Index. Differences in the refractive index, Δn, of solutions of PS49K in cyclohexanone from that of the pure solvent were measured at 25 °C and $\lambda = 632.8$ nm by using a KMX16 differential refractometer (Chromatix). A plot of Δn as a function of concentration, c, was well fitted by a straight line of $\Delta n/(c/\text{wt}\%) = 1.40 \times 10^{-3}$ ($0 \le c \le 7.5$ wt %).

Cell. A porous glass bead (L for PS49K, PS90K, and PS288K; M for PS25K) was fixed in a fluorometer cell (UVONIC, Type 23, 10 mm) by holding the lower half with a Teflon tubing. The tubing was then supported by a stainless steel rod at the center of the cell. Many holes were punctured through the side of the tubing to ensure a rapid exchange of the liquid in the tubing with the exterior solution when the polymer was added. Before addition of the polymer, an interferogram was recorded for a cell that contained ca. 1.6 g of cyclohexanone immersing the glass bead. A given amount of polymer was added to the cell at $t = 0$. The cell was hand-shaken for several minutes. Subsequently, the cell was enclosed in a tightly-capped polypropylene bottle placed on a 60 rpm orbital rotation stage. For each recording of the interferogram at a designated time, the cell was taken out of the bottle and placed in a cell holder at 25.0 °C for at least 30 min before the recording. After completion of the infusion experiment, the cell was washed several times with pure solvent for 4−7 days before it was used for the next concentration.

Interferometer. We used the interferometer constructed earlier.[3] The wavelength of the laser was $\lambda = 632.8$ nm. The image was recorded by a Hi-8 video camcorder (Sony CCD-FX710) and digitized by a Macintosh Centris 660AV (Apple Computer). Recording of a pair of interferograms (bead image and background image) was described earlier in detail.[3] Profile plotting function of NIH "Image 1.52" (available by anonymous FTP from zippy.nimh.nih.gov) was used for a rectangle selected.

Procedures of Image Analysis. Figure 2 is an example of bead images photographed before the polymer was added and at $t = 2.7$, 10.5, and 148 h, respectively, after the exterior concentration, c_E, of PS25K was raised from 0 to 50.6 mg/mL. The fringe pattern within the bead image in (a) is displaced left, because of a lower index of refraction in the exterior solvent compared with that of silica. In contrast, other fringe patterns are displaced right, indicating that the average refractive index in the silica bead is lower. A highly distorted pattern in (b), compared with the one in (d), implies a nonuniform distribution of the polymer in the bead. The distortion diminished afterward. We intentionally employed a solvent with $n_S < n_G$ to allow a large swing in the displacement at short times compared to the one at $c_E = 0$. If $n_S \cong n_G$, then $\Delta x/\xi$ would be too large, and indexing of the dark fringes in the bead and in the background would be difficult, especially at short times. Also note that the interior fringes at the equator are parallel to the background fringes. Without sufficient holes in the supporting tubing, the pattern would be skewed, implying asymmetric concentration distribution in the porous silica with respect to the equator plane.

A rectangular bar of width 8 pixels was drawn on the bead image along the diameter perpendicular to the background fringes. A "profile plot" of NIH Image for the selected bar

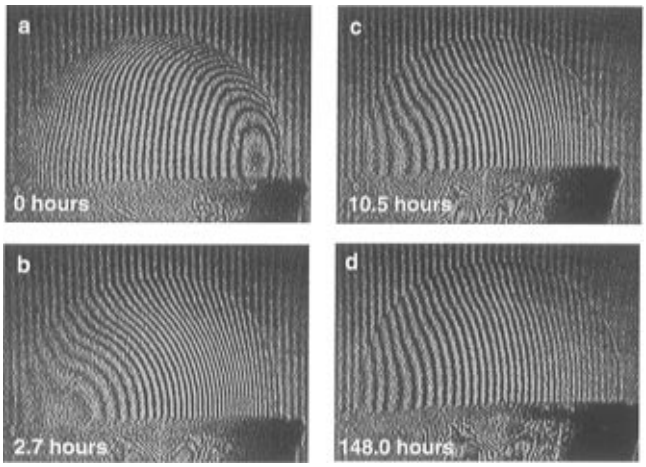

Figure 2. Example of bead images (a) before polymer was added and (b) 2.7, (c) 10.5, and (d) 148 h after the exterior concentration of PS25K was raised from 0 to 50.6 mg/mL.

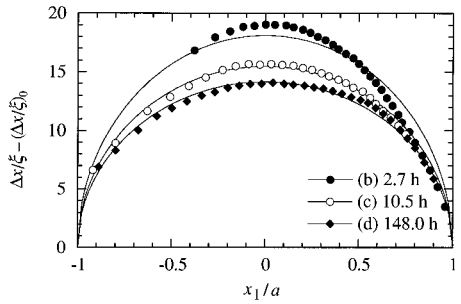

Figure 3. Plots of $(\Delta x/\xi) - (\Delta x/\xi)_0$ 2.7, 10.5, and 148 h after PS25K was added to the exterior solution.

generated an intensity profile as a function of the number of pixels from the left end of the bar. Each dark fringe was marked by its peak position, x_1 (in pixels), relative to the bead center. Two peaks were marked for a closed fringe. To record a background image, the cell holder was nudged down to pass the two beams through the exterior solution above the glass bead. An intensity profile was obtained for a rectangular bar at the same location as that used in the bead image. A displacement, Δx, was calculated for each of the dark fringes by comparing the two plots. The period ξ was calculated as the average across ca. 20 fringes in the background image.

In the analysis of the bead image before addition of the polymer, $(\Delta x/\xi)_0$ was fitted by a sixth-order polynomial as a function of x_1/a, where a is the half of the diameter of the bead image along the bar selected. The polynomial was used for $(\Delta x/\xi)_0$ in eq 6 for the bead images taken after the polymer was added. Symbols in Figure 3 show $\Delta x/\xi - (\Delta x/\xi)_0$ for the three interferograms in Figure 2b−d. Solid lines are best fit by an ellipse, $B(1 - (x_1/a)^2)^{1/2}$, with an adjustable parameter, B. Clearly, fitting is poor for (b) that showed skewed displacement of fringes. The good fitting for (d) indicates that the cross section at the equator is close to a circle.

To take into account a small deviation of the cross section from a circle, we evaluated the path length, l_1, as a function of x_1/a for the image at the longest time in each infusion experiment. We verified that the image did not change between two consecutive recordings interspaced by at least 2 days. Another sixth-order polynomial was used to fit $(\Delta x/\xi)_{eq} - (\Delta x/\xi)_0$. The polynomial was translated into an expression for l_1 by using the measured value of d. With the polynomial for l_1, $\overline{c_I}(x_1)$ was then obtained for the other images, where eq 6 was used. The results are shown in Figure 4. As polymer chains infuse into the interior of the porous glass bead and permeate the medium, $\overline{c_I}$ approaches $c_{I,eq}$ for all x_1/a. Then, eq 9 was used to fit $\overline{c_I}$. From ϕ_0, ϕ_2, ϕ_4, and ϕ_6 obtained, we calculated $c_I(r)$. The results are shown in Figure 9b by solid lines. Values at $r/a \gtrsim 0.9$ are not reliable because we do not have an expression for l_1 in that range.

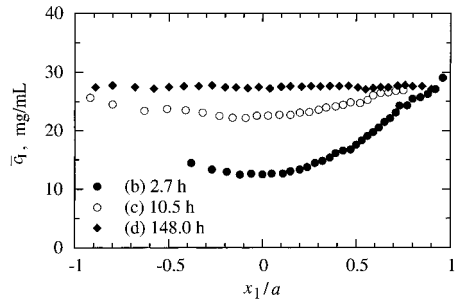

Figure 4. Plots of $\overline{c_I}$ as a function of x_1/a 2.7, 10.5, and 148 h after PS25K was added to the exterior solution.

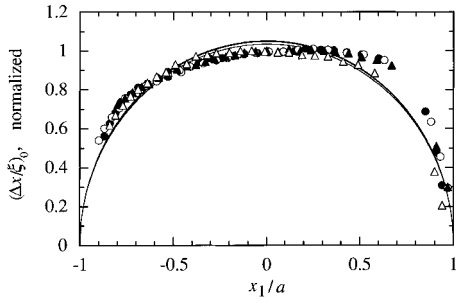

Figure 5. Plots of normalized $(\Delta x/\xi)_0$ for images taken on different occasions. The lines are the best fits by a semi-ellipse.

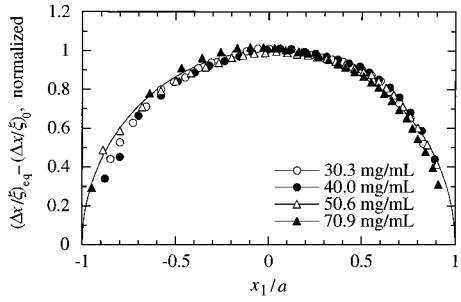

Figure 6. Plots of normalized $(\Delta x/\xi)_{eq} - (\Delta x/\xi)_0$ for images taken after the glass bead was equilibrated with solutions of various concentrations of PS25K. The lines are the best fits by a semi-ellipse.

The accuracy in $\Delta x/\xi$ is better than 0.1 in every interferogram. The largest source of error is in the estimate of x_1/a for each fringe. When the edges are not sharp on the bead image, there can be a systematic error in x_1/a. A more serious error occurs when small scars on the surface of the silica bead cause local distortion of the fringes. Nonsmoothness in the plot of $\overline{c_I}$ in Figure 4 is ascribed mostly to the local distortion and is responsible for the errors in $c_I(r)$.

Examination of Nonidealities. Equations 6 and 7 assume that ρ and n_G are uniform throughout the glass bead. We examine here how nonuniform ρ and n_G affect the fringe pattern. For this purpose, we prepared a pair of figures. Figure 5 shows plots of $(\Delta x/\xi)_0$ measured for bead M on four different occasions, normalized by the peak value of the polynomial fitting (not shown), as a function of x_1/a. Figure 6 shows plots of $(\Delta x/\xi)_{eq} - (\Delta x/\xi)_0$, normalized by the peak value of the elliptic fitting, for $c_E = 30.3$, 40.0, 50.6, and 70.5 mg/mL of PS25K. The solid lines in the two figures are the best fit by an ellipse centered at $x_1/a = 0$. As shown in the Appendix, spatial fluctuations in n_G cause a deviation in $(\Delta x/\xi)_0$ from a semi-elliptic trace, but not in $(\Delta x/\xi)_{eq} - (\Delta x/\xi)_0$. In contrast, spatial fluctuations in ρ affect both. So does the noncircular cross section. Comparison of the two figures indicates a deviation in the plots of $(\Delta x/\xi)_0$, but not in those of $(\Delta x/\xi)_{eq} - (\Delta x/\xi)_0$. The difference was similar for bead L. Therefore, we conclude that the porous glass beads used have spatial distributions in n_G sufficiently large to distort $(\Delta x/\xi)_0$. The distribution in ρ is negligible, however, and the cross

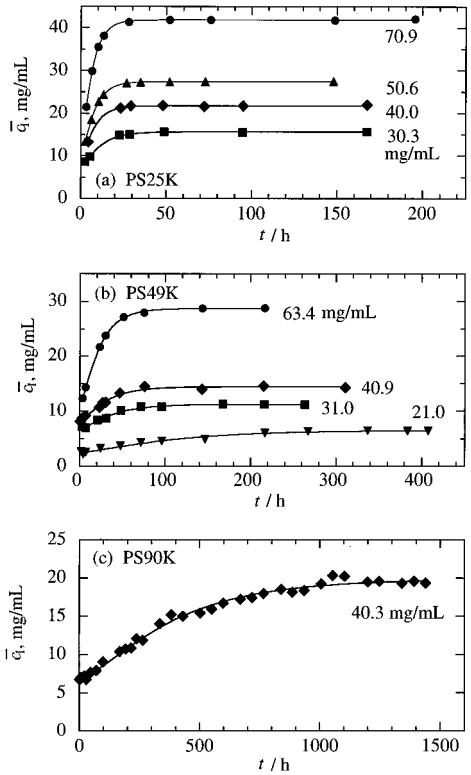

Figure 7. Average concentration along a diameter of a glass bead, $\overline{c_I}(0)$, plotted as a function of time after (a) PS25K, (b) PS49K, and (c) PS90K was added. The exterior concentration is indicated adjacent to each plot. The solid lines are the best fits by an equation derived by assuming rapid penetration followed by diffusion-limited permeation.

section is close to a circle. Thus, use of eqs 6 and 7 to estimate $\overline{c_I}(x_1)$ and $c_I(r)$ is justified.

Center of the Bead Image. We carried out infusion experiments to measure the interior concentration profile $c_I(\mathbf{r})$, at different times t for the initial condition $c_I(\mathbf{r})|_{t=0} = 0$. If marginal pores (those at the edge of the glass bead) establish equilibrium with the surrounding solution immediately after the polymer is added, the boundary condition is given as $c_I(|\mathbf{r}| = a) = c_{I,eq}$. The solution of the diffusion equation (with a constant and uniform diffusion coefficient, D_I) is given as

$$c_I(r)/c_{I,eq} = 1 + 2A\sum_{n=1}^{\infty}(-1)^n \frac{a}{n\pi r} \sin\frac{n\pi r}{a} \exp(-(n\pi/a)^2 D_I t) \quad (10)$$

where $r \equiv |\mathbf{r}|$ and $A = 1$. At the center of the bead image, the displacement of the fringe gives an average of $c_I(\mathbf{r})$ along the diameter as

$$\overline{c_I}(0)/c_{I,eq} = 1 + 2A\sum_{n=1}^{\infty}(-1)^n S_n \exp(-(n\pi/a)^2 D_I t) \quad (11)$$

where $S_n \equiv \int_0^{n\pi} x^{-1} \sin x \, dx$ is always positive.

Symbols in Figure 7 show $\overline{c_I}(0)$ as a function of t for PS25K (a), PS49K (b), and PS90K (c). The values of c_E are indicated adjacent to each plot. For all of the measurements (except for PS288K), there was a rapid increase of $\overline{c_I}(0)$ in $t \lesssim 2$ h, followed by a gradual increase and a level-off to $c_{I,eq}$ over a long time. We fitted (not shown) the transients by eq 11 with two adjustable parameters, $c_{I,eq}$ and D_I, but with A fixed to 1. For PS25K, the fitting worked well for all of c_E. This result suggests that marginal pores quickly establish equilibrium with the surrounding solution, and the polystyrene molecules spread throughout the porous medium following the diffusion equation with an effective diffusion coefficient D_I. For PS49K and PS90K, however, fitting was poor, regardless of c_E. The initial rapid increase and the gradual increase at later stages cannot be ascribed to different terms in eq 11.

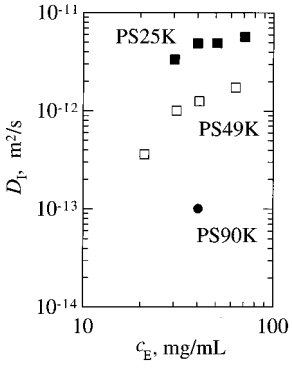

Figure 8. Intrapore diffusion coefficient, D_I, plotted as a function of c_E, the polymer concentration exterior to the pore.

Table 2. Diffusion Coefficients in the Porous Silica Bead

polymer	c_E, mg/mL	D_I, m²/s	$\eta D_I/kBT$, μm^{-1}
PS25K	30.3	3.4×10^{-12}	1.6
PS25K	40.0	4.9×10^{-12}	2.4
PS25K	50.6	4.9×10^{-12}	2.4
PS25K	70.9	5.7×10^{-12}	2.8
PS49K	21.0	3.6×10^{-13}	0.18
PS49K	31.0	1.0×10^{-12}	0.50
PS49K	40.9	1.3×10^{-12}	0.62
PS49K	63.4	1.7×10^{-12}	0.86
PS90K	40.3	1.0×10^{-13}	0.050

For PS288K at $c_E = 40.9$ mg/mL, $\overline{c_I}(0)$ remained unchanged for 240 h after an initial stepwise increase to ca. 6.7 mg/mL (not shown). We then terminated the experiment.

The stepwise increase in $c_I(r)$ is equivalent to the initial condition $c_I(\mathbf{r})|_{t=0} = c_{I,eq}(1 - A)$ with $A < 1$. The solution of the diffusion equation is given by eq 10, and eq 11 remains the same. We fitted $\overline{c_I}(0)$ by allowing A to change. The fitting is shown by solid lines in Figure 7. The apparent diffusion coefficients D_I thus obtained are listed in Table 2. The value of D_I is almost proportional to the slope of a straight line that fits $\ln(1 - \overline{c_I}(0)/c_{I,eq})$ as a function of t (not shown).

The height of the stepwise increase, $c_{I,eq}(1 - A)$, was in the range of 6.4−6.8 mg/mL for all of c_E in PS25K and PS90K. In PS49K, the height was in the same range for $c_E = 31.0$ mg/mL, but smaller for $c_E = 21.0$ mg/mL and slightly larger for $c_E = 40.9$ and 63.4 mg/mL.

Figure 8 is a plot of D_I as a function of c_E for the three fractions of polystyrene. For both PS25K and PS49K, infusion is faster at higher concentrations. The dependence of D_I on the molar mass, compared at the same c_E, is steep. In particular, D_I of PS90K is less than one-tenth of that of PS49K.

To compare the diffusion coefficients thus estimated with the results of dynamic light scattering (DLS),[14] we calculated $\eta D_I/k_B T$, where $\eta = 2.02$ cP is the viscosity of cyclohexanone at $T = 25$ °C, and k_B is the Boltzmann constant. In the DLS experiments, mutual diffusion coefficients of polystyrene fractions in a porous glass bead with the same nominal pore diameter were measured. The surrounding solution had a sufficiently low concentration of the polymer. 2-Fluorotoluene ($\eta = 0.55$ cP) was used as a solvent, and the temperature was 37.8 °C to attain the optimal index-matching. We interpolated their diffusion coefficient data and evaluated $\eta D_I/k_B T$ as 3.66, 1.52, and 0.547 μm^{-1} for PS25K, PS49K, and PS90K, respectively. The values of $\eta D_I/k_B T$ obtained in the interferometry are smaller than those estimated in DLS. We will discuss the difference in the next section.

The equilibrium partition coefficient, $K = c_{I,eq}/c_E$, in the zero c_E extrapolate was found to be 0.47 and 0.25 for PS25K and PS49K, respectively. These are larger than the values estimated for a Gaussian chain of the same R_g in a pore of radius $R_p = 7.5$ nm (see Table 1). Conversely, we estimated the effective pore radius that gives the estimated partition coefficients. The radius was found to be 20 and 18 nm for PS25K and PS49K, respectively. The concentration dependence of K

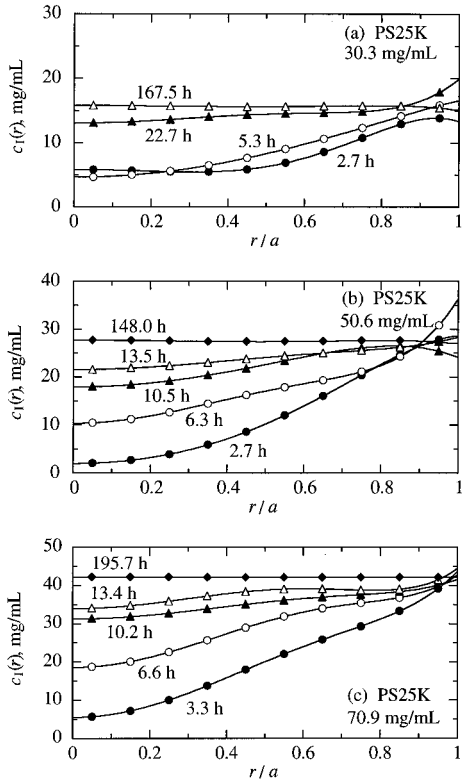

Figure 9. Concentration profile in the porous glass bead in the course of infusion of PS25K for c_E = (a) 30.3, (b) 50.6, and (c) 70.9 mg/mL. The time is indicated adjacent to each curve. Symbols distinguish the curves.

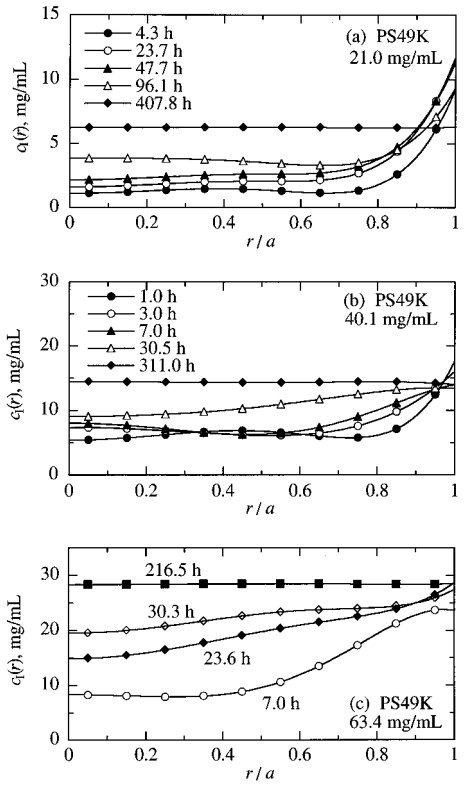

Figure 10. Concentration profile in the porous glass bead in the course of infusion of PS49K for c_E = (a) 21.0, (b) 40.1, and (c) 63.4 mg/mL.

was found to be small for both fractions. These results alone suggest either that porous glass beads used have a large pore size distribution or that low molar mass components of the polymer enter the pores easily.

Distribution of Concentration. Equations 8 and 9 were used to deconvolute $\overline{c_I}(x_1)$ into $c_I(r)$. Figure 9 shows $c_I(r)$ as a function of r/a for c_E = 30.3, 50.6, and 70.9 mg/mL of PS25K at different times. Figure 10 uses c_E = 21.0, 40.1, and 63.4 mg/mL of PS49K, and Figure 11 is for c_E = 40.3 mg/mL of PS90K. Use of a fourth-order polynomial (even terms only) in eq 9, in general, produced a concentration profile similar to the one shown in the figure. In contrast, fitting by an eighth-order polynomial exaggerated experimental errors in the image analysis to produce large fluctuations in $c_I(r)$. Negative concentration gradients are unphysical. We therefore used a sixth-order polynomial fitting for all of the analysis.

In the infusion of PS25K, the concentration increased initially at the edge of the bead, followed by a gradual propagation of the increase toward the center of the bead. The trend is evident at all concentrations. In the infusion of PS90K, in contrast, $c_I(r)$ increased almost in unison throughout the medium, although c_I was slightly higher toward the edge at intermediate times. The infusion of PS49K has characteristics between those of PS25K and PS90K. At c_E = 21.0 mg/mL, $c_I(r)$ increased almost uniformly, except for the edge. At 63.4 mg/mL, the transient was similar to that of PS25K.

The profile of $\overline{c_I}(x_1)$ was almost flat for PS288K with little change in the height in the range of time measured. We therefore did not perform deconvolution.

The stepwise increase in c_I, observed in the radial average $\overline{c_I}(0)$, was seen in the entire medium and was almost uniform. The rapid increase is not due to migration of polymer chains into the pores near the bead surface. Apparently, some polymer chains penetrate deeply the porous medium much more quickly than other chains. We could not, however, trace permeation transients for those quickly penetrating chains.

As we noted earlier, polymer chains have to first enter the porous medium to infuse. The temporal change of the concentration profile allows us to compare the time scale of permeation with that of entrance for those chains that occupy the medium more slowly toward equilibrium. In the infusion of PS90K, the polymer chains spread throughout the porous medium as soon as they enter the pores from the surrounding solution, on the time scale of the latter. The rate-limiting process was the entrance into the marginal pores. In the infusion of PS25K, in contrast, intrapore diffusion of polymer chains already in the interior of the porous medium was rate-limiting. We can see a cross-over in PS49K, from entrance-limited infusion at low concentrations to permeation-limited infusion at higher concentrations.

When the concentration profile shows an almost uniform increase, as in Figure 11, fitting of the profiles measured at different times by eq 10 does not work. The slow entrance can be taken into account by assuming, for instance, that the marginal pores reach the equilibrium with the surrounding solution at a rate constant of Γ, i.e., $c_I(a) = c_{I,eq}(1 - A\exp(-\Gamma t))$. The solution of the diffusion equation for the boundary condition and the initial condition $c_I(\mathbf{r})|_{t=0} = c_{I,eq}(1 - A)$ is given as

$$c_I(r)/c_{I,eq} = 1 + A\left[2\sum_{n=1}^{\infty}(-1)^n \frac{1}{1-(n\pi/ka)^2}\frac{a}{n\pi r}\sin\frac{n\pi r}{a} \times \exp(-(n\pi/a)^2 D_I t) - \frac{a\sin kr}{r\sin ka}\exp(-\Gamma t)\right] \quad (12)$$

with $k = (\Gamma/D_I)^{1/2}$. When $\pi/a \ll k$ (fast entrance), eq 12 reduces to eq 10. When $\pi/a \gg k$ (slow entrance), the concentration profile shows a uniform increase:

$$c_I(r)/c_{I,eq} = 1 - A\exp(-\Gamma t) \quad (13)$$

In general, the overall rate of increase in $\overline{c_I}(0)$ lies between $(\pi/a)^2 D_I$ and Γ. The apparent diffusion coefficient, D_I, in Table 2 is strongly affected by Γ when the infusion is entrance-limited. We then fitted the concentration profiles by eq 12. A variable A (<1) accounts for a rapid and uniform increase in short times. The simultaneous fitting of all of the profile plots by eq 12 works well when the infusion is strongly entrance-limited, such as in 21.0 mg/mL of PS49K and 40.3 mg/mL of

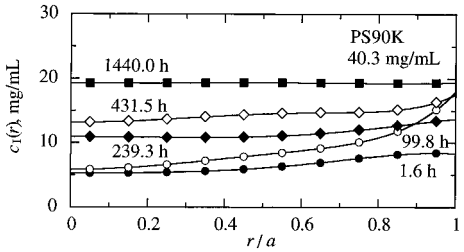

Figure 11. Concentration profile in the porous glass bead in the course of infusion of PS90K for $c_E = 40.3$ mg/mL.

Table 3. Fitting Results

polymer	c_E, mg/mL	D_I, m^2/s	Γ, s^{-1}	A	$\eta D_I/kBT$, μm^{-1}
PS49K	21.0	2.1×10^{-12}	8.5×10^{-3}	0.74	1.0
PS90K	40.3	5.0×10^{-13}	3.2×10^{-3}	0.67	0.25

PS90K, producing a finite Γ. The results are shown in Table 3. The overall fitting is still not as good as we expected, probably because of nonlinear diffusion in the presence of a large chemical potential gradient and a concentration-dependent diffusion coefficient.

Discussion

(1) Short-Time Penetration. We consider the mechanism of the uniform, stepwise increase in $c_I(r)$ shortly after adding the polymer to the solvent. Possible mechanisms are given below.

Distribution of Molar Mass. Polystyrene standards are not free from the distribution of molar mass. When a solvent-filled porous medium is equilibrated with a solution of the polymer, low molar mass components, if any, are forced to enter the pores by the high osmotic pressure exerted by the majority components.[24] The pore total volume is only about 1/1000 of the exterior volume in the cell. If a small fraction of the polymer has a molar mass less than half of M_p, for instance, the fraction will instantaneously occupy the pores (helped also by faster diffusion of these components in the porous medium), resulting in a nearly stepwise and uniform increase in $c_I(r)$. Once the porous medium is filled with polymer chains that find it easy to infuse, these chains begin to repel newly entering chains. Thus, the majority components can fill the pores only slowly. The time constants for the quickly infusing components and the rest will be greatly different when the latter finds it difficult to enter the pores, as is the case for PS90K. The percentage of the stepwise increase will be smaller as c_E increases, because of a limited space available in the porous medium. Experimental errors in the plots of $c_I(r)$ are, however, as large as one-tenth of $c_{I,eq}$ and do not allow quantitative discussion of the percentage.

Distribution of Pore Size. For the presence of larger pores to account for the rapid and uniform increase, the medium must have a uniform distribution of channels of a larger diameter, and the diameter must be much greater compared with a typical diameter in other pores. The two rates observed are too widely different to ascribe the rapid increase solely to the presence of larger pores in the glass beads. Furthermore, the interconnected network structure of the porous medium precludes the presence of larger channels.

Distribution of the Chain Dimension. At a given time, some polymer chains have a dimension smaller than the average. Simple calculations show that the standard deviation of R_g^2 of a Gaussian chain is about 0.516 of $\langle R_g^2 \rangle$. The dimension is changing on the time scale of τ_1, the relaxation time of the first normal mode in the Rouse−Zimm model. If those polymer chains enter the pores and reach a portion of a larger cavity (such as junctions of pore channels) before the chain explores different conformations, the chain is likely to stay in the pore to permeate further into the interior of the porous medium. Two time scales are relevant here. One is τ_1, given as $\tau_1 \approx \eta \langle R_g \rangle^3/k_B T$.[25] The other is τ_p, the time needed for the chain to diffuse into one of the most shallow junctions. It is estimated as $\tau_p \approx L^2/D_I$, where L is the depth of the junctions. We note that L is a few times the size of R_p. Then, $\tau_p \approx R_p^2/D_I$. The ratio of the two time scales is found to be $\tau_p/\tau_1 \approx (D_{E0}/D_I)(R_p/\langle R_g \rangle)^2$, where we used $D_{E0} \approx k_B T/\eta \langle R_g \rangle$, with D_{E0} the diffusion coefficient of the polymer chain in the dilute exterior solution. Note that D_{E0}/D_I is greater than unity and is an increasing function of $\langle R_g \rangle/R_p$. DLS studies[14] showed that $D_E/D_I \approx M_p \approx (\langle R_g \rangle/R_p)^{5/3}$ in the relevant range of M_p. Therefore, $\tau_p/\tau_1 \approx (R_p/\langle R_g \rangle)^{1/3}$. The entrance will not be rejected if $\tau_p < \tau_1$, a situation more likely for chains with a larger $\langle R_g \rangle$. Although the fraction of chains temporarily with $R_g < R_p$ decreases as $\langle R_g \rangle$ increases, it is possible for some chains to enter the pore and move forward deeply into the pore. Once inside the medium, they permeate quickly with a diffusion coefficient temporarily greater than D_I. Infusion of polymer chains by this mechanism will continue until they occupy all of the larger cavities. Once large cavities are filled with polymer chains, these chains begin to repel newly entering chains. Thus, there will be a marked contrast in the rate of infusion.

If the third mechanism is the case, it may impair the resolution of GPC. The partitioning at short time scales favors high molar mass components much more than it does at long-time equilibrium that presumably occurs at every plate in the column.

The first and third mechanisms are in agreement with the experimental results. The measured height of the stepwise increase can also be explained by either of the two mechanisms. Further studies, including those of computer simulation, are needed to identify the mechanism.

(2) Comparison of Entrance and Permeation. Here we compare theoretically the rate of entrance and the rate of permeation, assuming that polymer chains are initially absent in the porous medium. At low concentrations, the rate, Γ, of the entrance of a polymer chain of molar mass M into a given pore is proportional to the partition coefficient. Then, for a sufficiently long chain, $\Gamma \propto \exp(-fM)$,[26] where f is a constant. In contrast, short chains can enter the pores easily. The rate of permeation is proportional to the diffusion coefficient D_I in the pore that follows $D_I \propto M^{-b}$, where b was found experimentally[14] to be $1 < b < 2$. As M increases, Γ decreases more rapidly than D_I decreases. Thus infusion of polymer chains will be permeation-limited when M is small and entrance-limited when M is large. The conclusion agrees with our observation of infusion at low concentrations.

As the exterior concentration c_E increases, Γ will change, but little change is expected for D_I, because initially the concentration is low in the pore. For chains to enter the pore, they must first escape from other chains in the exterior solution. Therefore, the entrance will be impeded by slower self-diffusion of entangled polymer chains on the one hand but will be facilitated, on the other hand, by a larger difference in the chemical potential of the polymer chain between the exterior and

the interior of the porous medium. We consider the concentration effect for entangled chains and unentangled chain separately.

When the chains are entangled, the difference, $\Delta\mu$, in the chemical potential between the exterior and the interior solutions increases as $(\Delta\mu - \Delta\mu_0)/k_BT \approx (c_E/c^*)^{5/4}$ with reference to the dilute solution value $\Delta\mu_0$, because the osmotic pressure Π increases as $\Pi \propto (c_E/c^*)^{9/4}$. The latter relationship was derived in the scaling theory[26] and later confirmed by experiments.[27] The reptation theory[25] tells us that the self-diffusion coefficient D_E in the exterior solution decreases as $D_E \approx D_{E0}(c_E/c^*)^{-3/2}$ in the semidilute solution. The decrease in D_E is greater than the increase in $\Delta\mu$. The entanglement will slow down the entrance.

The argument above applies to highly entangled chains only. Comparison of the osmotic pressure data[27] and the self-diffusion coefficients obtained[28] by using forced Rayleigh scattering shows that, at around the overlap concentration, the increase in $\Pi M/(cRT)$ is greater than the decrease in D_E/D_{E0}, where R is the gas constant. Repulsive interactions between chains make the entrance faster before the entanglement slows it down eventually at higher concentrations.

When the chains are short and not entangled, the increase in $\Delta\mu$ will be greater than the decrease in D_E. It is known for polystyrene that the second virial coefficient A_2 scales as $A_2 \approx M^{-0.2}$ and deviates upward for $M < 10^4$.[23] This property contributes to increasing $\Delta\mu$. The absence of entanglement makes the decrease in D_E moderate. Thus, the higher concentration will facilitate the entrance. The observed faster entrance of PS25K and PS49K into the pore at higher concentrations is probably due to the larger difference in $\Delta\mu$.

In the preceding section, we found that our estimate of $\eta D_I/k_BT$ is much smaller than the one estimated in DLS. The difference persists even after the slow entrance is taken into account. We ascribe the difference to the presence of polymer chains in the pore as newly permeating chains spread in the porous medium. They should have delayed majority components' spreading into the interior of the porous glass bead.[15,16]

Concluding Remarks

We have shown that analysis of the fringe pattern along the diameter of a porous glass bead makes it possible to distinguish the entrance from the permeation in the infusion of polymer chains into the porous medium. With the analysis of the displacement at the center of the bead image alone, it is difficult to distinguish the two events. Further improvement in the accuracy and the resolution will make the space-resolved interferometry able to analyze diffusion processes including nonlinear transport processes in a porous medium.

When polymer chains are highly entangled, the rate of entrance will depend on the pore size relative to the tube diameter (of the tube model) in the surrounding solution, in addition to the partition coefficient and the curvilinear diffusion coefficient of chains along the tube. We may be able to use a solid porous medium as a microprobe of the tube diameter.

Future extensions include use of porous materials of geometry other than spheres. In particular, rod-shaped porous glasses are available in a better symmetry than that of a spherical porous glass piece used in this contribution. A similar image analysis can be employed. It may be also possible to apply the interferometry to trace infusion of molecules into a fully swollen hydrogel. Swelling and contraction of the gel may also be studied by this method.

Acknowledgment. Partial support by NSF Young Investigator Award is gratefully acknowledged. We also thank Dr. H. Wechsler for financial support.

Appendix

Let us first assume that n_G is not uniform but ρ is uniform:

$$n_I(\mathbf{r}) = (1 - \rho)n_G(\mathbf{r}) + \rho n_S + \rho(dn/dc)\, c_I(\mathbf{r}) \quad \text{(A1)}$$

Then the path difference is

$$\int_A^B [n_E - n_I(\mathbf{r})]\, d\mathbf{r} = l_1[(n_S - \overline{n_G})(1 - \rho) + (dn/dc)(c_E - \rho\overline{c_I})] \quad \text{(A2)}$$

The measurements of Δx at $c_E = 0$ and at equilibrium with a polymer solution of $c_E > 0$ give

$$(\Delta x/\xi)_0 = (l_1/\lambda)(n_S - \overline{n_G})(1 - \rho) \quad \text{(A3)}$$

and

$$(\Delta x/\xi)_{eq} - (\Delta x/\xi)_0 = (l_1/\lambda)(dn/dc)(c_E - \rho c_{I,eq}) \quad \text{(A4)}$$

respectively. Note that eq A4 does not contain $\overline{n_G}$. Fluctuations in n_G does not affect eq A4 or eq 7. The plots of $(\Delta x/\xi)_{eq} - (\Delta x/\xi)_0$ as a function of x_1 should be on semi-ellipses for different values of c_E. Since $\overline{n_G}$ is a function of x_1, the deviation from the semi-ellipse should be seen in the plots of $(\Delta x/\xi)_0$.

Next, we assume that ρ is not uniform but n_G is uniform:

$$n_I(\mathbf{r}) = (1 - \rho(\mathbf{r}))n_G + \rho n_S + \rho(\mathbf{r})(dn/dc)\, c_I(\mathbf{r}) \quad \text{(A5)}$$

Then the path difference is

$$\int_A^B [n_E - n_I(\mathbf{r})]\, d\mathbf{r} = l_1[(n_S - n_G)(1 - \bar{\rho}) + (dn/dc)(c_E - \overline{\rho c_I})] \quad \text{(A6)}$$

The measurements of Δx at $c_E = 0$ and at equilibrium with a polymer solution of $c_E > 0$ give

$$(\Delta x/\xi)_0 = (l_1/\lambda)(n_S - n_G)(1 - \bar{\rho}) \quad \text{(A7)}$$

and

$$(\Delta x/\xi)_{eq} - (\Delta x/\xi)_0 = (l_1/\lambda)(dn/dc)(c_E - \bar{\rho}c_{I,eq}) = (l_1/\lambda)(dn/dc)c_E(1 - K\bar{\rho}) \quad \text{(A8)}$$

respectively. As opposed to fluctuations in n_G, those in ρ affect $(\Delta x/\xi)_0$ and, to a lesser degree, $(\Delta x/\xi)_{eq}$. Note that $K \cong 0.6$ for the present system.

References and Notes

(1) Teraoka, I. *Prog. Polym. Sci.* **1996**, *21*, 89.
(2) Giddings, J. C. *Unified Separation Science*; John Wiley: New York, 1991.
(3) Teraoka, I. *Macromolecules* **1996**, *29*, 2430.
(4) Daoud, M.; de Gennes, P. G. *J. Phys. (Paris)* **1977**, *38*, 85.
(5) Teraoka, I.; Langley, K. H.; Karasz, F. E. *Macromolecules* **1993**, *26*, 287.
(6) Guillot, G. *Macromolecules* **1987**, *20*, 2600.
(7) Deen, W. M. *AIChE J.* **1987**, *33*, 1409.

(8) Davidson, M. G.; Deen, W. M. *Macromolecules* **1988**, *21*, 3474.
(9) Kathawalla, I. A.; Anderson, J. L. *Ind. Eng. Chem. Res.* **1988**, *27*, 866.
(10) Kathawalla, I. A.; Anderson, J. L.; Lindsey, J. S. *Macromolecules* **1989**, *22*, 1215.
(11) Bishop, M. T.; Langley, K. H.; Karasz, F. E. *Phys. Rev. Lett.* **1986**, *57*, 1741.
(12) Bishop, M. T.; Langley, K. H.; Karasz, F. E. *Macromolecules* **1989**, *22*, 1220.
(13) Easwar, N.; Langley, K. H.; Karasz, F. E. *Macromolecules* **1990**, *23*, 738.
(14) Guo, Y.; Langley, K. H.; Karasz, F. E. *Macromolecules* **1990**, *23*, 2022.
(15) Zhou, Z.; Teraoka, I.; Langley, K. H.; Karasz, F. E. *Macromolecules* **1994**, *27*, 1759.
(16) Teraoka, I.; Zhou, Z.; Langley, K. H.; Karasz, F. E. *Macromolecules* **1996**, *29*, 37.
(17) Aven, M. R.; Cohen, C. *Polymer* **1990**, *31*, 778.
(18) Rotstein, N. A.; Lodge, T. P. *Macromolecules* **1992**, *25*, 1316.
(19) Pajevioć, S.; Bansil, R.; Koňák, C. *Macromolecules* **1993**, *26*, 305.
(20) Matsukawa, S.; Ando, I. *Macromolecules* **1996**, *29*, 7136.
(21) Schlick, S.; Pilař, J.; Kweon, S.-C.; Vacik, J.; Gao, Z.; Labsky, J. *Macromolecules* **1995**, *28*, 5780.
(22) Gao, Z.; Pilař, J.; Schlick, S. *J. Phys. Chem.* **1996**, *100*, 8430.
(23) Huber, K.; Bantle, S.; Lutz, P.; Burchard, W. *Macromolecules* **1985**, *18*, 1461.
(24) Teraoka, I.; Zhou, Z.; Langley, K. H.; Karasz, F. E. *Macromolecules* **1993**, *26*, 3223.
(25) Doi, M.; Edwards, S. F. *The Theory of Polymer Dynamics*; Clarendon Press: Oxford, 1986.
(26) de Gennes, P. G. *Scaling Concepts in Polymer Physics*; Cornell Univ. Press: Ithaca, NY, 1979.
(27) Noda, I.; Kato, N.; Kitano, T.; Nagasawa, M. *Macromolecules* **1981**, *14*, 668.
(28) Léger, L.; Hervet, H.; Rondelez, F. *Macromolecules* **1981**, *14*, 1732.

MA9704065